Universidade de São Paulo

Biblioteca Digital da Produção Intelectual - BDPI

Departamento de Física e Ciências Materiais - IFSC/FCM Artigos e Materiais de Revistas Científicas - IFSC/FCM

2011-07

Optical spectroscopy of Nd3+ ions in a nanostructured glass matrix

Journal of Luminescence, Amsterdam : Elsevier, v. 131, n. 7, p. 1401-1406, July 2011
http://www.producao.usp.br/handle/BDPI/50029

Downloaded from: Biblioteca Digital da Produção Intelectual - BDPI, Universidade de São Paulo

Journal of Luminescence 131 (2011) 1401–1406

Contents lists available at ScienceDirect

Journal of Luminescence

journal homepage: www.elsevier.com/locate/jlumin

Optical spectroscopy of Nd^{3+} ions in a nanostructured glass matrix

E.O. Serqueira [a], N.O. Dantas [a], V. Anjos [b], M.A. Pereira-da-Silva [c,d], M.J.V. Bell [b,*]

[a] Laboratório de Novos Materiais Isolantes e Semicondutores (LNMIS), Instituto de Física, Universidade Federal de Uberlândia, 38400-902 Uberlândia-MG, Brazil
[b] Grupo de Espectroscopia de Materiais, Departamento de Física, Universidade Federal de Juiz de Fora, 36036-330 Juiz de Fora-MG, Brazil
[c] Instituto de Física de São Carlos, USP, São Carlos, SP 13560-250, Brazil
[d] Centro Universitário Central Paulista, UNICEP, São Carlos, SP 13563-470, Brazil

ARTICLE INFO

Article history:
Received 7 November 2010
Received in revised form
1 March 2011
Accepted 11 March 2011
Available online 21 March 2011

Keywords:
Nd^{3+}
CdS
Glasses
Luminescence
Judd–Ofelt

ABSTRACT

This paper presents the optical characterization of Nd^{3+} ions in nanostructured SiO_2–Na_2CO_3–Al_2O_3–B_2O_3 (SNAB) CdS glass, synthesized by fusion. Radiative properties of the glass were determined by absorption, luminescence spectroscopy and lifetime measurements. Nd^{3+} emission enhancement and quenching were investigated in the presence of CdS nanocrystals. Nd^{3+}-emission quenching was attributed to upconversion mechanisms and nonradiative processes such as multiphonon decay and energy transfer, while the Nd^{3+}-emission enhancement was due to energy transfer from the CdS nanocrystals. Changes in the chemical environment around CdS nanocrystals were also confirmed by Judd–Ofelt calculations.

© 2011 Elsevier B.V. All rights reserved.

1. Introduction

Glass systems codoped with rare earth (RE) ions and semiconductor nanocrystals (NCs) have attracted great research interest because of their applications in optical systems [1–3]. The influence of semiconductor NCs on the radiative properties of RE ions has been demonstrated, particularly with Eu^{3+}, Tb^{3+}, Er^{3+}, Pr^{3+} and Nd^{3+} [4–6].

The importance of the research relates to the possibility of energy transfer from semiconductor nanocrystals (NCs) to rare earth ions, which may result in enhancement of the rare earth luminescence. The effect is due to the higher absorption cross-section of semiconductor NCs when compared to those of rare earth ions [7]. Particularly, the absorption band of CdS NCs can be tuned according to CdS NCs dimensions. It means that resonance with Nd^{3+} bands can be achieved, increasing the probability of energy transfer to Nd^{3+}. As the absorption bands of CdS NCs are broader than the ones of Nd^{3+}, it ensures a better match in wavelength of the pump sources (usually diode lasers) for the achievement of opto-electronic devices, such as laser active media [8,9], optical amplifiers [10], microchips [11] and planar waveguides due to their emission in the near infrared range at 1060 nm [3,12,13].

SNAB glass was chosen as host to CdS because it is suitable for the growth of high quality CdS and due to its transparency to the UV through near-IR, where energy transfer processes take place and the most important Nd^{3+} absorption and emission bands occur. SNAB host has been previously investigated. Ref. [6] exposes the energy transfer process from CdS NCs to Nd^{3+} ions in the present samples. Moreover, a study of the thermal properties was performed and revealed that CdS nanoparticles reduce the thermal diffusivity of the samples [14].

Nevertheless there is a lack of data from analysis, based on the Judd–Ofelt Theory, regarding the spectroscopic properties of RE ions embedded in glass systems codoped with semiconductor NCs [15–20]. It is well known that this type of analysis produces the so called Judd–Ofelt parameters Ω_λ ($\lambda=2, 4, 6$), which can be used to find spontaneous emission probability, branching probability (branching ratio), emission cross-section, radiative lifetime and effective linewidth. These parameters can also be used to predetermine if an RE ion host material is suitable for optical device applications [15,21–24].

The main objective of this research was to evaluate the spectroscopic fluorescence parameters of Nd^{3+} ions embedded in a SiO_2–Na_2O–Al_2O_3–B_2O_3 glass system in the presence of CdS NCs, as a function of thermal annealing time. Electronic dipole transitions are permitted due to the mixture of opposite parity wave-functions in the $4f^N$ configuration of rare earth ions.

According to the Judd–Ofelt Theory, electric dipole oscillator strength, between initial $|f^n[\alpha SL]J\rangle$ and final states $|f^n[\alpha' S'L']J'\rangle$, is given by

$$f^{ED}(J,J') = \frac{8\pi^2 mc}{3h}\frac{1/\lambda}{(2J+1)}\chi\sum_{\lambda=2,4,6}\Omega_\lambda\left|\langle f^n[\alpha SL]J\left|U^{(\lambda)}\right|f^n[\alpha' S'L']Jf^n[\alpha' S'L']J'\rangle\right|^2, \quad (1)$$

where m is the electron mass, c the speed of light, $1/\lambda$ is the wave number, h the Planck constant, J the angular moment of the initial

* Corresponding author.
E-mail address: mjbell@fisica.ufjf.br (M.J.V. Bell).

0022-2313/$ - see front matter © 2011 Elsevier B.V. All rights reserved.
doi:10.1016/j.jlumin.2011.03.032

state $|f^n[\alpha SL]J\rangle$, $\chi=(n^2+2)^2/9n$ the central field correction factor, n the refractive index of the wave number ε, Ω_λ the Judd–Ofelt intensity parameter and $|\langle f^n[\alpha SL]J||U^{(\lambda)}||f^n[\alpha' S'L']J'\rangle|^2$ represents the reduced matrix elements of the tensor operator. It is important to mention that quadrupole oscillator strength is not considered since its contribution is negligible [25].

The Judd–Ofelt intensity parameters, Ω_λ ($\lambda=2,4$ and 6), are calculated from experimental oscillator strength using the following expression

$$f^{exp}(\lambda)=\frac{mc}{\pi e^2 N}\int \alpha(\lambda)d\lambda \quad (2)$$

where N is RE ion concentration per unit volume (ions/cm^3) and $\alpha(\lambda)$ is the absorption coefficient at wavelength λ. When magnetic dipole transitions (f^{MD}) are present, experimental oscillator strength (f^{exp}) can be expressed as $f^{exp}=f^{ED}+f^{MD}$.

Radiative transition rates (A) can be obtained from the expression

$$A(J,J')=\frac{64\pi^4 e^2}{3h(2J+1)\lambda^3}\chi\sum_{\lambda=2,4,6}\Omega_\lambda\left|\langle f^n[\alpha SL]J||U^{(\lambda)}||f^n[\alpha' S'L']J'\rangle\right|^2 \quad (3)$$

The emission branching ratio (β) for transitions originating from the initial manifold (in this case the $^4F_{3/2}$ level) can be calculated from the radiative transition probabilities $A(J,J')$ using the equation [26]

$$\beta\left(^4F_{3/2}\rightarrow{}^4I_{J'}\right)=\frac{A\left(^4F_{3/2}\rightarrow{}^4I_{J'}\right)}{\sum_{J'}A\left(^4F_{3/2}\rightarrow{}^4I_{J'}\right)} \quad (4)$$

where the summation includes each J' ($J'=9/2$, 11/2, 13/2 and 15/2).

To compare theoretical data obtained from Eq. (4) with experimental data, the ratio of the integral of an emission band, $\int I(\lambda)d\lambda$, to the sum of the integrals of all emission bands, $\sum\int I(\lambda)d\lambda$, is calculated. This results in the experimental emission branching ratio represented by

$$\beta_{exp}=\frac{\int I(\lambda)d\lambda}{\sum\int I(\lambda)d\lambda} \quad (5)$$

The stimulated emission cross-section for the $^4F_{3/2}\rightarrow{}^4I_{J'}$ transition is obtained from [22]

$$\sigma_{em}\left(^4F_{3/2}\rightarrow{}^4I_{J'}\right)=\frac{\lambda_p^4}{8\pi c n\Delta\lambda_{eff}}A\left(^4F_{3/2}\rightarrow{}^4I_{J'}\right), \quad (6)$$

where λ_p is the peak emission wavelength, c the speed of light in vacuum, n the refractive index at each peak emission wavelength and $\Delta\lambda_{eff}$ is the effective linewidth, given by [26]

$$\Delta\lambda_{eff}=\frac{\int I(\lambda)d\lambda}{I_{max}}, \quad (7)$$

where I_{max} is the maximum intensity at fluorescence emission peaks and $I(\lambda)$ is the experimental fluorescence line shape.

Nanoparticle size can be estimated using a simple confinement model based on effective mass approximation [27]. In this case, the energy of the lowest exciton state in NCs of radius R smaller than the exciton Bohr radius a_B can be estimated by

$$E_{conf}(R)=E_g+\frac{\hbar^2\pi^2}{2\mu R^2}-1.8\frac{e^2}{\varepsilon R}, \quad (8)$$

where E_g is the material (bulk) energy gap, μ is the reduced effective mass, e is the elementary charge and ε is the dielectric constant. Eq. (8) can be used to estimate the average size of CdS nanocrystals. For CdS, the following parameters were used: $E_g=2.58$ eV, $\mu=0.154m_o$ (where m_o is the mass of a free electron) and $\varepsilon=5.7$ [27,28].

2. Experimental details

A SNAB glass matrix with nominal composition $40SiO_2$–$30Na_2CO_3$–$1Al_2O_3$–$29B_2O_3$ (mol%) was synthesized by the fusion method both undoped and doped with Nd^{3+} ions and bulk CdS. The molar composition of the codoped SNAB glasses is 39.527 SiO_2 . 29.645 Na_2CO_3 . 0.988 Al_2O_3 . 28.657 B_2O_3+0.73 CdS(bulk)+0.452 Nd_2O_3 (mol%), or SNAB+2[CdS (bulk)+Nd_2O_3] (wt%), considering the composition in wt%. These samples were synthesized in porcelain crucibles in a carbon rich atmosphere at 1300 °C for 15 min. Afterwards, the melt was rapidly cooled. In order to reduce non-homogeneities, the melt was manually rotated at least three times inside the crucible. This procedure has been seen to be efficient since the homogeneity of the samples, tested by absorption measurements at different points of the samples, show the same optical density. Then, samples of the doped SNAB glass matrix were heated at 560 °C for 0, 2, 4, 6, 8 and 10 h to induce nucleation and growth of CdS NCs by diffusion of Cd^{2+} and S^{2-} ions resulting from the fusion of bulk CdS.

Optical absorption spectra (OA) were obtained using a Shimadzu UV-3600 spectrophotometer. Photoluminescence spectra (PL) were obtained using a He–Cd ($\lambda_{ex}=325$ nm) laser and a photomultiplier operating in the range 350–900 nm. Lifetimes of the $^4F_{3/2}$ state of the Nd^{3+} ion were obtained through luminescence decay of the Time Resolved PL (TRPL) spectra ($^4F_{3/2}\rightarrow{}^4I_{9/2}$) using a He–Cd ($\lambda_{ex}=325$ nm) laser. All measurements were performed at room temperature.

The atomic force microscopy (AFM) images were obtained using a Multimode Nanoscope IIIa (Digital Instruments—Veeco). All AFM images were obtained at room temperature under ambient conditions.

3. Results and discussion

Fig. 1 shows the DTA thermogram of SNAB glass. It exhibited a vitreous transition temperature at about 529 °C and crystallization temperature not well defined at around 600 °C, which indicates that SNAB glass presents high stability against crystallization. It can be concluded that SNAB is thermally stable at room temperature, suggesting that it could present high mechanical resistance required for laser hosts.

Fig. 2 displays atomic force microscopy image for SNAB+2[CdS (bulk)+Nd_2O_3] (wt%) sample heated at 560 °C for 10 h. The image clearly shows the nanostructured nature of these SNAB systems. The histogram indicates the formation of nanocrystals (CdS dots) with mean size about 4.7 nm, as well as particles of approximately 7 nm. These larger particles are expected to demonstrate bulk-like behavior. Larger nanosized particles, averaging 50–100 nm can also be seen in the AFM image.

Fig. 3a shows the OA spectra of CdS dots grown in the doped SNAB matrices, heated at 560 °C for increasing annealing times. Two OA bands can be observed: one is sensitive to thermal treatments and displays redshift and the other remains unchanged at about 480 nm (bulk gap energy $E_{g(CdS)}=2.58$ eV). The OA band with redshift displays quantum confinement properties and is associated with the NC emission. The line shapes and intensities of Nd^{3+} ion OA bands remain constant and unaffected by thermal treatment. These results provide further evidence that the doping ions were not incorporated into CdS NCs during growth. Finally, transition probabilities of Nd^{3+} ions change when a hosting medium transforms from amorphous to crystalline [29,30]. In this case, there is a decrease in band intensity at 580 nm and the Stark structure of the bands at 740, 810 and 880 nm was modified due to crystal field influence [31]. The findings of this study indicate that Nd^{3+} ions remained immersed in the SNAB matrix during thermal treatment.

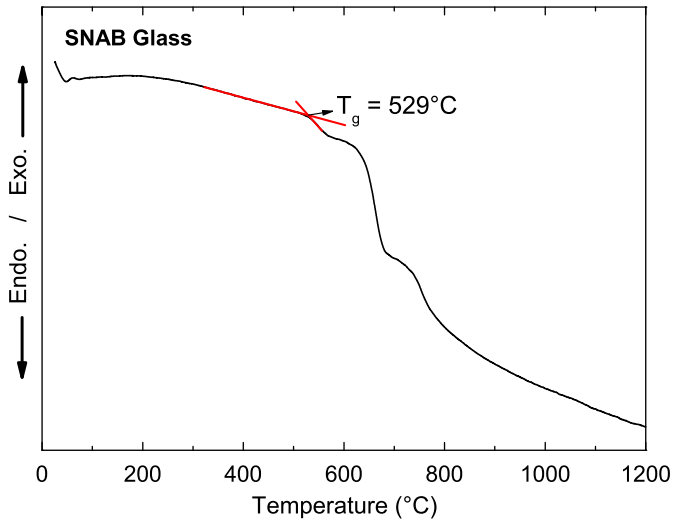

Fig. 1. DTA thermogram of the SNAB host. Vitreous transition temperature is 529 °C and crystallization temperature, not well defined, around 600 °C.

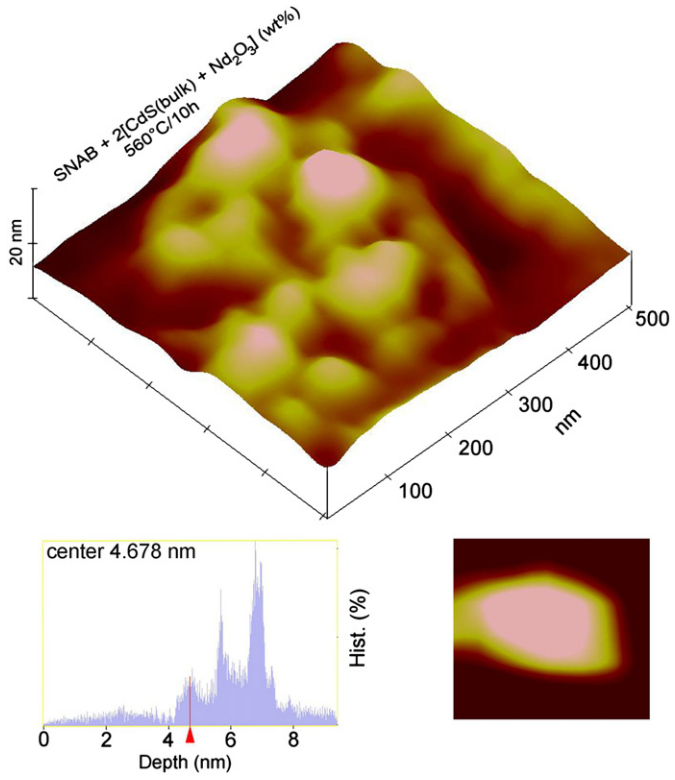

Fig. 2. Atomic force microscopy of the SNAB+2[CdS (bulk)+Nd_2O_3] (wt%) sample heated at 560 °C for 10 h.

Fig. 3b shows PL of the samples. The broad emission in the range 500–900 nm originates from the CdS NCs, and it is dependent on the size of NCs, size dispersion and heat treatment time. It can be noted that there is a shift to higher wavelengths as the time of heat treatment increases, indicating the average size of NCs increased [6]. In addition, no redshift is detected in the peak absorption energies of Nd^{3+} ions and the emission band valleys of CdS NCs. Instead, they remain centered exactly in the absorption positions of the Nd^{3+} ions. Therefore, these results provide evidence of efficient energy transfer from NCs to neodymium embedded in the SNAB matrix, as previously investigated in Ref. [6]. It was shown that the

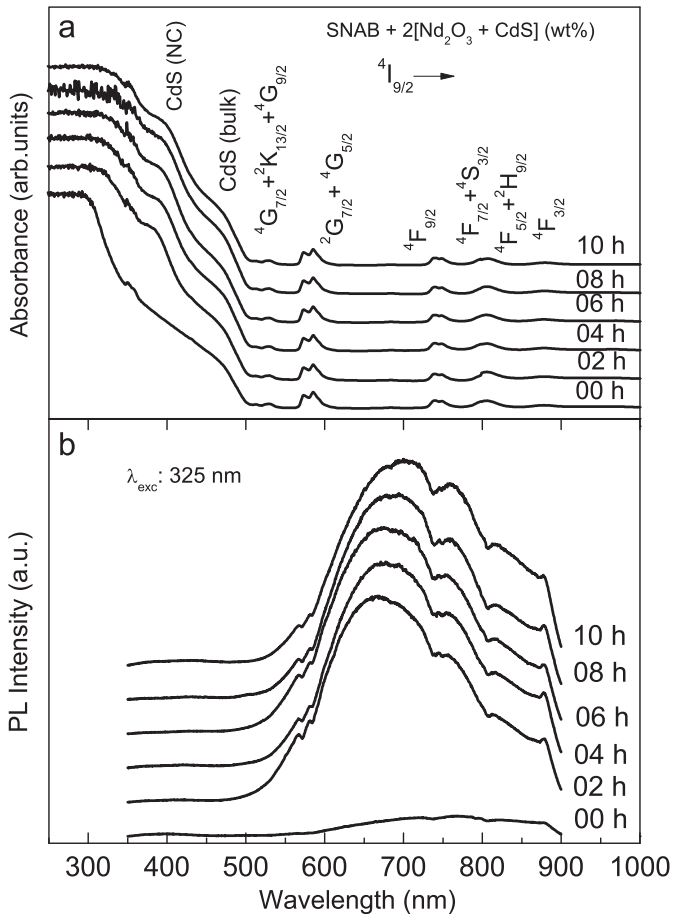

Fig. 3. (a) OA spectra and (b) PL of the SNAB+2[CdS (bulk)+Nd_2O_3] (wt%) samples heated at 560 °C for 0, 2, 4, 6, 8 and 10 h.

luminescence of CdS NC strongly overlaps the Nd^{3+} electronic transitions labeled $^4I_{9/2}\rightarrow{}^2G_{7/2}$, $^4I_{9/2}\rightarrow{}^4G_{5/2}$, $^4I_{9/2}\rightarrow{}^4F_{9/2}$, $^4I_{9/2}\rightarrow{}^4F_{7/2}+{}^4S_{3/2}$, $^4I_{9/2}\rightarrow{}^4F_{5/2}+{}^2H_{9/2}$ and $^4I_{9/2}\rightarrow{}^4F_{3/2}$. Consequently, the emission bands presented valleys that were centered exactly at the Nd^{3+} absorption peaks. Such an effect was attributed to energy transfer from CdS NCs to doping ions. Moreover, the increase in average nanocrystal size leads to an increasing overlap between the luminescence resonances and the $^4F_{3/2}$ Nd^{3+} energy states.

Fig. 4a shows the Judd–Ofelt intensity parameters and the spectroscopic quality parameter χ ($\chi=\Omega_4/\Omega_6$) for the Nd^{3+} ions in the SNAB+2[CdS (bulk)+Nd_2O_3] (wt%) samples heated at 560 °C for 0, 2, 4, 6, 8 and 10 h. It can be seen that Ω_2 decreases with treatment time indicating that CdS NC growth increased symmetry around Nd^{3+} ions. In this study, Ω_2 decreased slightly with thermal treatment time. In other words, the ligand field around the Nd^{3+} became more symmetric with time [32,33]. The JO Ω_4 parameter is related to the long range covalency effects of the network [34–36]. This parameter increased as a function of treatment time, indicating the increase of long range effects [34,35]. The value of the Ω_6 parameter, in turn, is proportional to the rigidity of the host [37]. The literature shows that NdF_3 samples demonstrate increased glass rigidity in glass-ceramics, indicating improved mechanical properties [37]. In this study, Ω_6 values were constant for the SNAB+2[CdS (bulk)+Nd_2O_3] (wt%) samples heated at 560 °C for 0, 2, 4, 6, 8 and 10 h indicating constant rigidity. The spectroscopic quality parameter χ is shown in Fig. 4b. This parameter increased steadily from 1.6 to 2.3, which indicates that the heat treatment elevated the spectroscopic quality of the SNAB+2[CdS (bulk)+Nd_2O_3] (wt%) samples when

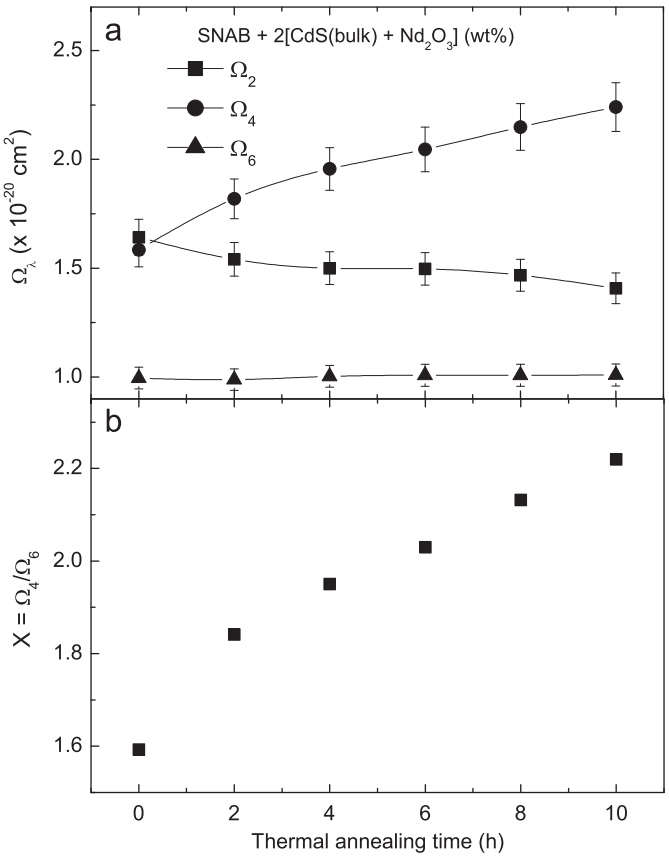

Fig. 4. (a) JO intensity parameters (Ω_λ) and (b) spectroscopic quality parameter ($\chi=\Omega_4/\Omega_6$) of Nd^{3+} ions in the SNAB+2[CdS (bulk)+Nd_2O_3] (wt%) samples heated at 560 °C for 0, 2, 4, 6, 8 and 10 h.

heated at 560 °C for 0, 2, 4, 6, 8 and 10 h. It is important to stress that emission intensity from the $^4F_{3/2}$ level can be completely characterized by the ratio of the intensity parameters Ω_4 and Ω_6. In the case of Nd^{3+}, this is due to the zero value of the reduced matrix elements $<{}^4F_{3/2}||U^2||{}^4I_J>$. According to the literature, if χ is higher than unity, the intensity of the $^4F_{3/2}\rightarrow{}^4I_{9/2}$ transition will be stronger than that of the $^4F_{3/2}\rightarrow{}^4I_{11/2}$ transition. For comparison purposes the χ values of the present glasses are similar to the ones of Nd^{3+} doped glasses [38,39], suggesting the possibility of laser emission from the $^4F_{3/2}\rightarrow{}^4I_{9/2}$ transition at 1.33 μm.

Higher values of Ω_4 with increasing treatment time suggest potential increases in the long range effects (e.g. increased packing density) of the nanostructured SNAB glass [34,35]. This fact affirms that more Nd cations dissolve in the glass matrix and the distance between adjacent Nd^{3+} cations diminishes. This probably increases the repulsive force between neighboring Nd cations and therefore increases Ω_4. This again reinforces the view that the Nd^{3+} ions were embedded in the glass matrix and not incorporated in CdS NCs.

Fig. 5 shows the $1/\Omega_6$ parameter of the Nd^{3+} ions in the SNAB+2[CdS (bulk)+Nd_2O_3] (wt%) samples heated at 560 °C for 0, 2, 4, 6, 8 and 10 h. It can be seen that $1/\Omega_6$ decreases with treatment time. Because of this, it is evident that heat treatment helped increase symmetry and reduce amorphization of the sample. In principle, high asymmetry in the ligand field increases Ω_2 and high covalency reduces Ω_6 [32,33]. Therefore, this result suggests that the Nd–O bond became less ionic as heat treatment time increased.

Fig. 6 shows the (a) theoretical and (b) trial branching ratios of the $^4F_{3/2}\rightarrow{}^4I_{9/2,\ 11/2,\ 13/2}$, transitions of the Nd^{3+} ions in the

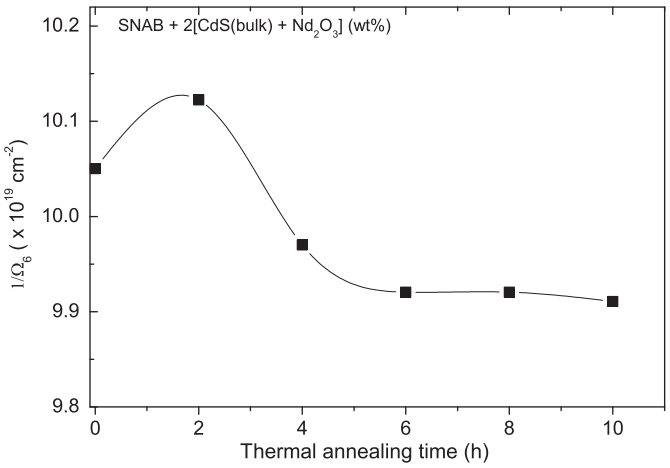

Fig. 5. Inverse of Ω_6 for the Nd^{3+} ions in the SNAB+2[CdS (bulk)+Nd_2O_3] (wt%) matrix heated at 560 °C for 0, 2, 4, 6, 8 and 10 h.

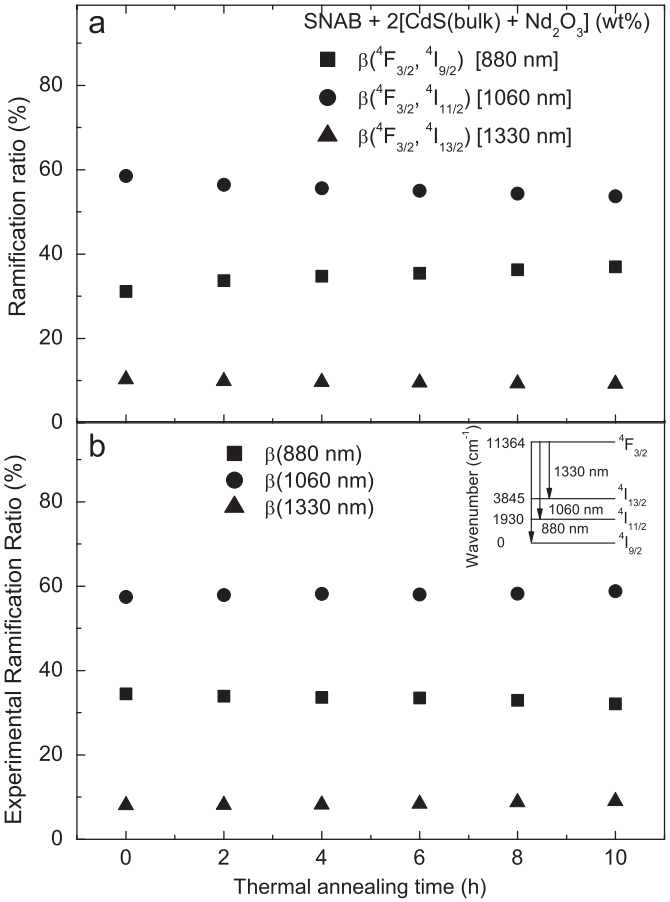

Fig. 6. (a) Theoretical and (b) experimental ramification ratio of the $^4F_{3/2}\rightarrow{}^4I_{9/2,\ 11/2,\ 13/2}$, electronic transitions of the Nd^{3+} ions in the SNAB+2[CdS (bulk)+Nd_2O_3] (wt%) samples heated at 560 °C for 0, 2, 4, 6, 8 and 10 h.

SNAB+2[CdS (bulk)+Nd_2O_3] (wt%) samples heated at 560 °C for 0, 2, 4, 6, 8 and 10 h. It can be seen that the calculations based on Eq. (4) are good approximations of those obtained from the areas under the emission bands in the luminescent emission spectra (Eq. (5)).

Fig. 7a shows the radiative and luminescence lifetime of the $^4F_{3/2}$ state of Nd^{3+} ions in the SNAB+2[CdS (bulk)+Nd_2O_3] (wt%) samples heated at 560 °C for 0, 2, 4, 6, 8 and 10 h. It can be seen that the luminescence lifetime is much less than radiative

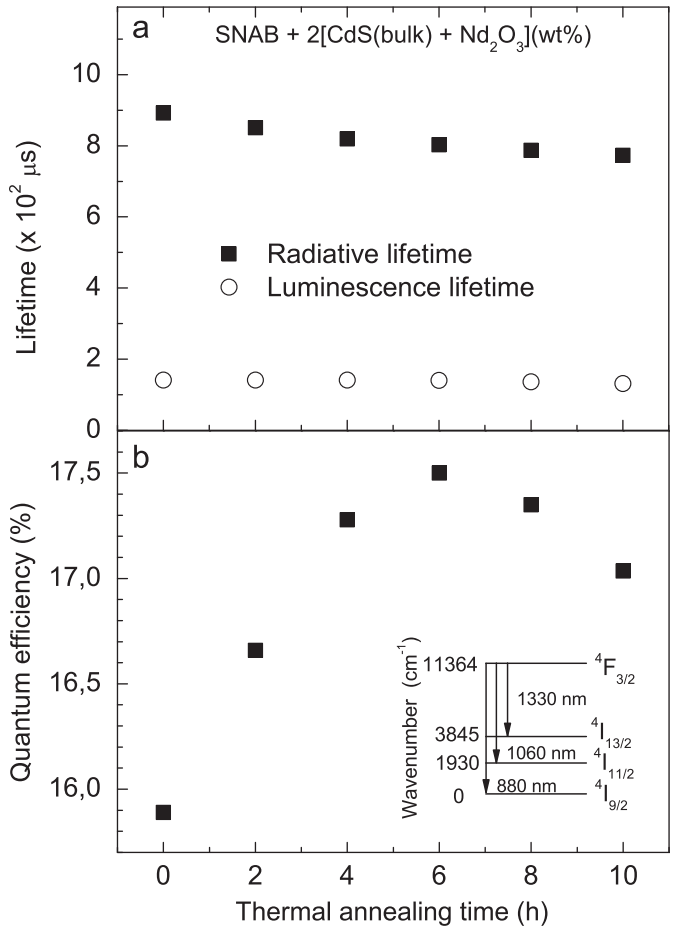

Fig. 7. (a) Radiative and luminescent lifetime of the $^4F_{3/2}$ state of Nd^{3+} ions in SNAB+2[CdS (bulk)+Nd_2O_3] (wt%) samples heated at 560 °C for 0, 2, 4, 6, 8 and 10 h. (b) Quantum efficiency of Nd^{3+} ions for the same samples.

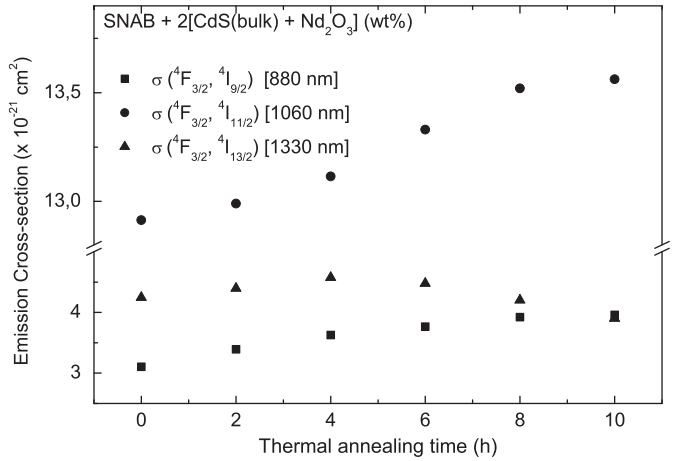

Fig. 8. Emission cross-section of the $^4F_{3/2} \rightarrow {}^4I_{9/2,\ 11/2,\ 13/2}$, electronic transition of Nd^{3+} ions in the SNAB+2[CdS (bulk)+Nd_2O_3] (wt%) samples heated at 560 °C for 0, 2, 4, 6, 8 and 10 h.

lifetime. This can be explained by assuming that nonradiative processes occurred such as multiphonon decay, energy transfer between Nd^{3+} ions and radiative and/or nonradiative transfer to CdS NCs. It can be seen that these NC emissions greatly overlap the absorption bands of the Nd^{3+} ions. The ratio of the luminescent to radiative lifetimes results in the quantum emission efficiency seen in Fig. 7b. The maximum quantum efficiency was obtained with 6 h of heat treatment.

Fig. 8 shows an emission cross-section of the $^4F_{3/2} \rightarrow {}^4I_{9/2,\ 11/2,\ 13/2}$ transitions of the Nd^{3+} ions in the SNAB+2[CdS (bulk)+Nd_2O_3] (wt%) samples heated at 560 °C for 0, 2, 4, 6, 8 and 10 h. It can be seen that the emission cross-sections of the $^4F_{3/2} \rightarrow {}^4I_{9/2}$, $^4F_{3/2} \rightarrow {}^4I_{11/2}$ and $^4F_{3/2} \rightarrow {}^4I_{13/2}$ transitions increase with heat treatment time and after 4 h of treatment, only the $^4F_{3/2} \rightarrow {}^4I_{13/2}$ section decreases. It appears that the emission cross-section of the $^4F_{3/2} \rightarrow {}^4I_{11/2}$ transition, at 1060 nm, is greater than the others and reaches a maximum of 1.36×10^{-20} cm^2.

Few studies can be found in the literature that use the Judd–Ofelt Theory to look at the influence of NC presence on RE ions and on the spectroscopic properties of RE ions. A study by Haldar and Patra [40] investigates rises in emissions of Eu^{3+} in the presence of Au nanoparticles. This study demonstrated a significant rise in the Ω_2 parameter when nanoparticles are present in the system. Kassab et al. [41] have also used JO parameters to predict spectroscopic properties in ZnO–TeO_2–Yb/Tm glass with silver nanoparticles.

It was concluded that the optical properties of neodymium ions can be influenced when embedded in a SNAB glass matrix nanostructured with CdS NCs. In this study, it was found that the thermal treatment of SNAB+2[CdS (bulk)+Nd_2O_3] (wt%) samples heated at 560 °C for 0, 2, 4, 6, 8 and 10 h increased relative quantum efficiency and emission section influence. In addition, Judd–Ofelt calculations demonstrated the influence of CdS NCs on the optical properties of Nd^{3+}. We believe that these results may inspire further investigation of this system for possible device applications, in particular lasers operating at 1.33 μm.

Acknowledgement

The authors acknowledge the financial support from the Brazilian agencies CNPq, FAPEMIG and CAPES.

References

[1] J.A. Moon, D.T. Schaafsma, Fiber Integrat. Opt. 19 (2000) 201.
[2] J.S. Sanghera, I.D. Aggarwal, J. Non-Cryst. Solids 256-257 (1999) 6.
[3] R.R. Gonçalves, J.J. Guimarães, J.L. Ferrari, L.J.Q. Maia, S.J.L. Ribeiro, J. Non-Cryst. Solids 354 (2008) 4846.
[4] L. Bokatial, S. Rai, J. Lumin. 130 (2010) 1857.
[5] B. Julian, J. Planelles, E. Cordoncillo, P. Escribano, P. Aschehoung, C. Sanchez, B. Viana, F. Pellé, J. Mater. Chem. 16 (2006) 4612.
[6] N.O. Dantas, E.O. Serqueira, A.P. Carmo, M.J.V. Bell, V. Anjos, G.E. Marques, Opt. Lett. 35 (2010) 1329.
[7] G. Ehrhart, B. Capoen, O. Robbe, F. Beclin, Ph. Boy, S. Turnell, M. Bouazaoui, Opt. Mater. 38 (2008) 1595.
[8] M.K. Chong, A.P. Abiyasa, K. Pita, S.F. Yu, Appl. Phys. Lett. 93 (2008) 151105.
[9] R.J. Reeves, C. Polley, J.S. Choi, J. Lumin. 129 (2009) 1673.
[10] A. Mussot, M. Le Parquier, B. Berrier, M. Perard, P. Szriftgiser, Opt. Commun. 282 (2009) 988.
[11] J. Sulc, H. Jelínková, K. Nejezchleb, V. Skoda, Opt. Mater. 30 (2007) 50.
[12] O. Péron, C. Duverger-Arfuso, Y. Jestin, B. Boulard, M. Ferrari, Opt. Mater. 31 (2009) 1288.
[13] A. Peled, A. Chiaxra, M. Nathan, M. Ferrrari, S. Ruschin, Appl. Phys. Lett. 92 (2008) 221104–1/3.
[14] E.O. Serqueira, N.O. Dantas, G.H. Silva, V. Anjos, M.J.V. Bell, M.A. Pereira-da-Silva, Chem. Phys. Lett. 504 (2011) 67.
[15] B.R. Judd, Phys. Rev. 127 (1962) 750.
[16] G.S. Ofelt, J. Chem. Phys. 37 (1962) 511.
[17] A. Majchrowski, L.R. Jaroszewicz, M. Swirkowicz, R. Miedzinski, M. Piasecki, I.V. Kityk, A. Wojciechowski, M.G. Brik, Mater. Lett. 64 (2010) 295.
[18] A. Agarwal, I. Pal, S. Sanghi, M.P. Aggarwal, Opt. Mater. 32 (2009) 339.
[19] Y. Luo, B. Chen, W. Wu, X. Yu, Q. Yan, Q. Zhang, J. Lumin. 129 (2009) 1309.
[20] S. Yu, Z. Yang, S. Xu, J. Fluoresc., (in press).
[21] N.O. Dantas, E.S.F. Neto, R.S. Silva, D.R. Jesus, F. Pelegrini, Appl. Phys. Lett. 93 (2008) 193115-1.
[22] W.T. Carnall, P.R. Fields, K. Rajnak, J. Chem. Phys. 49 (1968) 4424.
[23] S.S. Babu, R. Rajeswari, K. Jang, C.E. Jin, K.H. Jang, H.J. Seo, C.K. Jayasankar, J. Lumin. 130 (2010) 1021.
[24] M. Seshadri, K.V. Rao, J.L. Rao, K.S.R.K. Rao, Y.C. Ratnakaram, J. Lumin. 130 (2010) 536.
[25] K.B. Yatsimirskii, N.K. Davidenko, Coord. Chem. Rev. 27 (1979) 223.

[26] J.H. Choi, A. Margaryan, A. Margaryan, F.G. Shi, J. Lumin. 114 (2005) 167.
[27] L.E. Brus, J. Chem. Phys. 80 (1984) 4403.
[28] P.E. Lippens, M. Lannoo, Phys. Rev. B 39 (1989) 10935.
[29] P. Schobinger-Papamantellos, P. Fischer, A. Niggli, E. Kaldis, V. Hildebrandt, J. Phys. C: Solid State Phys. 7 (1974) 2023.
[30] D. Turnbull, J. Appl. Phys. 21 (1950) 1022.
[31] M. Abril, J. Méndez-Ramos, I.R. Martín, U.R. Rodríguez-Mendoza, V. Lavín, A. Delgado-Torres, V.D. Rodríguez, P. Núñez, A.D.Lozano Gorrín, J. Appl. Phys. 95 (2004) 5271.
[32] S. Tanabe, T. Hanada, T. Ohyagi, N. Soga, Phys. Rev. B 48 (1993) 10591.
[33] S. Tanabe, J. Non-Cryst. Solids 259 (1999) 1.
[34] Y. Nageno, H. Takebe, K. Morinaga, J. Am. Ceram. Soc. 76 (1993) 3081.
[35] H. Takebe, Y. Nageno, K. Morinaga, J. Am. Ceram. Soc. 77 (1994) 2132.
[36] E.W.J.L. Oomen, A.M.A. van Dongen, J. Non-Cryst. Solids 111 (1989) 205.
[37] C.K. Jorgensen, R. Reisfeld, J. Less-Common Met. 93 (1983) 107.
[38] R. Balda, J. Fernandez, M.A. Arriandiag, J.M. Fernandez-Navarro, J. Phys.: Condens. Matter 19 (2007) 086223.
[39] E.O. Serqueira, N.O. Dantas, A.F.G. Monte, M.J.V. Bell, J. Non-Cryst. Solids 352 (2006) 3628.
[40] K.K. Haldar, A. Patra, Appl. Phys. Lett. 95 (2009) 063103.
[41] L.P.R. Kassab, L. Ferreira-Freitas, K. Ozga, M.G. Brik, A. Wojciechowski, Opt. Laser Technol. 42 (2010) 1340.